Manufacturing Rev. **7**, 39 (2020)

https://doi.org/10.1051/mfreview/2020037

Manufacturing Review
Available online at:
https://mfr.edp-open.org

RESEARCH ARTICLE OPEN ACCESS

Hydrothermal synthesis of $ZnTa_2O_6$, $ZnNb_2O_6$, $MgTa_2O_6$ and $MgNb_2O_6$ pseudo-binary oxide nanomaterials with anticorrosive properties

Mihaela Birdeanu[1,*], Mirela Vaida[1,*], and Eugenia Fagadar-Cosma[2]

[1] National Institute for Research and Development in Electrochemistry and Condensed Matter, 1 Plautius Andronescu Street, Timisoara 300224, Romania
[2] "Coriolan Drăgulescu" Institute of Chemistry of the Romanian Academy, 24 M. Viteazul Ave., Timisoara 300223, Romania

Received: 15 October 2020 / Accepted: 30 November 2020

Abstract. $ZnTa_2O_6$, $ZnNb_2O_6$, $MgTa_2O_6$ and $MgNb_2O_6$ pseudo-binary oxide nanomaterials were synthesized through the hydrothermal method at 250 °C. Obtained materials were characterized by X-ray diffraction, UV-VIS measurements, field emission-scanning electron microscopy and atomic force microscopy techniques. XRD results show that the single phases of $ZnTa_2O_6$, $ZnNb_2O_6$, $MgTa_2O_6$ and $MgNb_2O_6$ pseudo-binary oxides nanomaterials were obtained, no thermal treatment being required. The values for the optical band gap of each material are settled in the range 3.60–3.80 eV. The anticorrosion characteristics of the obtained compounds were also evaluated after deposition on carbon steel in 0.5 M Na_2SO_4 media by open circuit potential measurements and potentiodynamic polarization technique with Tafel representation. The inhibition efficiency of pseudo-binary oxides deposited on carbon steel electrode was in the range 37–59.17%, promising for improvement of the anticorrosion properties.

Keywords: Oxides / hydrothermal / band gap / corrosion inhibition / tafel curves

1 Introduction

Corrosion is one of the most studied processes because this affects everything around us. Corrosion inhibition represents a goal due to the damages that corrosion leads to the carbon steel equipment's and installations in a lot of industries, whose remedy implies financial and also time losses. To fight against this process, there were developed methods and techniques as: plating's of the steel's parts or the usage of different organic or inorganic corrosion inhibitors – which are often used to protect materials in different environments [1–6].

Corrosion inhibitors represent one of the most economical solutions used to prevent the corrosion. In the present paper, the developing and obtaining of corrosion inhibitors as: $ZnTa_2O_6$, $ZnNb_2O_6$, $MgTa_2O_6$ and $MgNb_2O_6$ pseudo-binary oxide nanomaterials are presented. It is known that until present, to obtain $ZnTa_2O_6$, $ZnNb_2O_6$, $MgTa_2O_6$ and $MgNb_2O_6$ pseudo-binary oxides nanomaterials, there were used synthesis methods as: solid-state method [7–12], sol-gel method [13], molten salt method [14,15], polymerized complex method [16], ceramic method [15,17] or other chemical routes [18–20]. The different methods of synthesis, which were used in obtaining these categories of pseudo-binary oxides materials, present some issues like: controlling the particle size and the surface areas, which must be resolved.

The present study presents the obtaining of $ZnTa_2O_6$, $ZnNb_2O_6$, $MgTa_2O_6$ and $MgNb_2O_6$ pseudo-binary oxides nanomaterials by using the hydrothermal method at 250 °C. Also, are presented results regarding structural, morphological, topographical and optical characterizations of the named materials, and the results regarding the corrosion inhibition efficiency for each obtained nanomaterial evaluated in 0.5 M Na_2SO_4 media.

2 Experimental

2.1 Materials and methods

The hydrothermal synthesis method was used to obtain the pseudo-binary oxide nanomaterials type: $ZnTa_2O_6$, $ZnNb_2O_6$, $MgTa_2O_6$ and $MgNb_2O_6$. The main challenge, by using this method, was to select the proper

*e-mail: mihaelabirdeanu@gmail.com; vaida.mirela@yahoo.com

Table 1. The starting materials used to obtain pseudo-binary oxide nanomaterials.

The pseudo-binary oxide nanomaterial	Precursor 1	Precursor 2	Molar ratio
$ZnTa_2O_6$	$Zn(CH_3COO)_2$ x $2H_2O$ (98%, Sigma-Aldrich)	Ta_2O_5 (99% Sigma-Aldrich)	1:1
$ZnNb_2O_6$		Nb_2O_5 (99%, Merck)	
$MgTa_2O_6$	$Mg(CH_3COO)_2$ x $4H_2O$ (99%, Sigma-Aldrich)	Ta_2O_5 (99% Sigma-Aldrich)	
$MgNb_2O_6$		Nb_2O_5 (99%, Merck)	

hydrothermal parameters (t, T), in order to achieve a successfully morphology and crystalline structure of the materials. Based also on a previously experience in obtaining anticorrosive materials by the hydrothermal method [21,22], the optimal hydrothermal parameters were chosen as it can be seen in Table 1. It was found that the anticorrosive materials $ZnTa_2O_6$, $ZnNb_2O_6$, $MgTa_2O_6$ and $MgNb_2O_6$ can be successfully synthesized at a 1:1 molar ratio of the used precursors for each material, at a temperature of 250 °C for 12 h. The pH values of the synthesis were fixed at 13, using NaOH (97%, Merck), resulting an alkaline medium.

Further, the obtained pseudo-binary oxide nanomaterials were deposited as thin layers (using the drop casting method in acetone medium), in different combinations on carbon steel electrode disks. The carbon steel disks, with 10 mm diameter and 2 mm thick, had the following chemical composition: 93.80% Fe; 4.81% Ni; 0.51% Co; 0.005% Cu; 0.19% P and 0.01% S. Before the drop casting depositions, the carbon steel disks were polished with emery paper and thus rinsed with double distilled water and degreased with ethanol. The modified carbon steel disks were used as working electrodes in the corrosion tests.

2.2 Apparatus

The phase identification of the synthesized nanomaterials was investigated by X-ray diffraction (XRD) on a X'pert Pro MPD X-ray diffractometer with monochromatic Cu Kα ($\lambda = 1.5418$ Å) on an incident radiation. For the morphological investigations regarding the obtained pseudo-binary oxides, field emission-scanning electron microscopy (SEM/EDAX) (Model INSPECT S) and atomic force microscopy (AFM) (Model NanoSurfEasyScan 2 Advanced Research) were used. The optical band gap for each pseudo-binary oxide nanomaterial was calculated by recording the difusse reflectance spectra at room temperature using an UV-VIS-NIR spectrometer Lambda 950.

A Voltalab potentiostat (Model PGZ 402) was used to perform the electrochemical measurements. The potentiostat was coupled with a three electrodes electrochemical cell comprising: a platinum wire as a counter electrode, a saturated calomel electrode as the reference electrode and the working electrodes consisting in bare or drop casting modified carbon steel disks (OL). The potentiodynamic polarization measurements were recorded by sweeping the potential from −1.3 to −0.6 V at a scan rate (ν) of 1 mV/s at room temperature (23 °C). Before the polarization, the open circuit potential (OCP) of the modified electrodes was monitored for 30 min. For the corrosion tests a 0.5 M Na_2SO_4 solution was used.

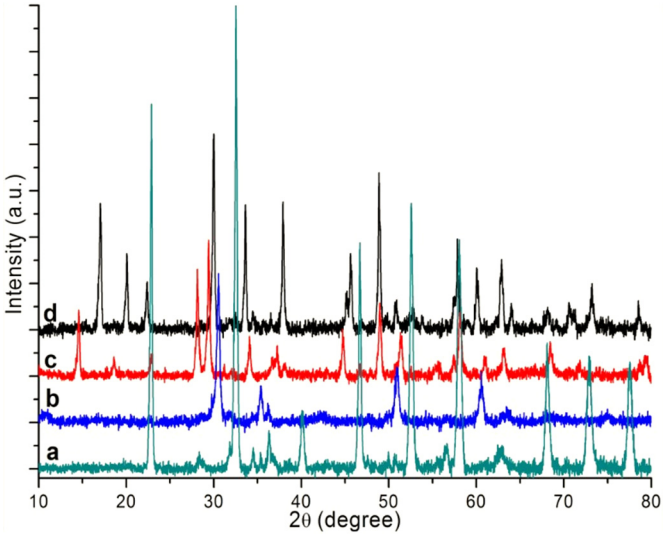

Fig. 1. The XRD patterns of: (a) $ZnTa_2O_6$, (b) $ZnNb_2O_6$, (c) $MgTa_2O_6$ and (d) $MgNb_2O_6$ materials prepared through the hydrothermal method.

3 Results and discussion

3.1 Structural and morphological properties

The X-ray diffraction patterns recorded at room temperature in the 2θ range of 10–80° are presented in Figure 1 for: (a) $ZnTa_2O_6$, (b) $ZnNb_2O_6$, (c) $MgTa_2O_6$ and (d) $MgNb_2O_6$. These patterns are showing that the phases of the materials do appear and the peaks are indexed with: the JCPDS no. 01-076-1826 for $ZnTa_2O_6$ where the main diffraction peak appears at 32.56°, JCPDS No. 01-076-1827 for $ZnNb_2O_6$ with the main diffraction peak settled at 30.49°, JCPDS No. 01-084-1679 for $MgTa_2O_6$ main diffraction peak at 29.37° and JCPDS No. 01-088-0708 for $MgNb_2O_6$ where the main diffraction peak is settled at 30.03°. Samples (a), (b) and (d) belong to the orthorhombic space group *Pbcn* (no. 60), while sample (c) belongs to the tetragonal space group *P42/*mnm (no. 136).

The morphology of the resulting pseudo-binary oxide nanomaterials (as powders, before the depositions) and the

formation of the agglomerates are represented in Figure 2. It is to be mentioned that for the pseudo-binary oxide nanomaterials which contain Ta, are preserved cubic shapes beside irregular shapes (Fig. 2a and 2c, while in the morphology of the pseudo-binary oxides with Nb content, the accicular shapes of the agglomerates is preserved (Fig. 2b and 2d). From the EDAX images for $ZnTa_2O_6$, $ZnNb_2O_6$, $MgTa_2O_6$ and $MgNb_2O_6$ nanomaterials (Fig. 3) it can be observed that only the specific lines for Zn, Mg, Ta, Nb and O are presented.

Topographic analysis for the surface of the obtained nanomaterials was perfomed using atomic force microscopy. The recorded images are presented for each nanomaterial in Figure 4a–d.

To calculate the surface roughness for each sample of material, the NanoSurf EasyScan 2 computer program and the following equations were used [23]:

$$S_a = \frac{1}{MN}\sum_{k=0}^{M-1}\sum_{l=0}^{N-1}|z(x_k, y_l)| \quad (1)$$

for the average roughness and

$$S_q = \sqrt{\frac{1}{MN}\sum_{k=0}^{M-1}\sum_{l=0}^{N-1}(z(x_k, y_l))^2} \quad (2)$$

for the mean square root roughness, where N and M represent the number of the crystal axes x and y respectively; z represents the average height of crystallites; x_k and y_l are the maximum and minimum deviations from the average crystallite.

In Table 2 are presented the calculated values for the measured areas of the obtained nanomaterials. The measurements were taken in the non contact mode using a scan size of $1\,\mu m \times 1\,\mu m$. The measured area at the surface for each material was 1.30 pm^2.

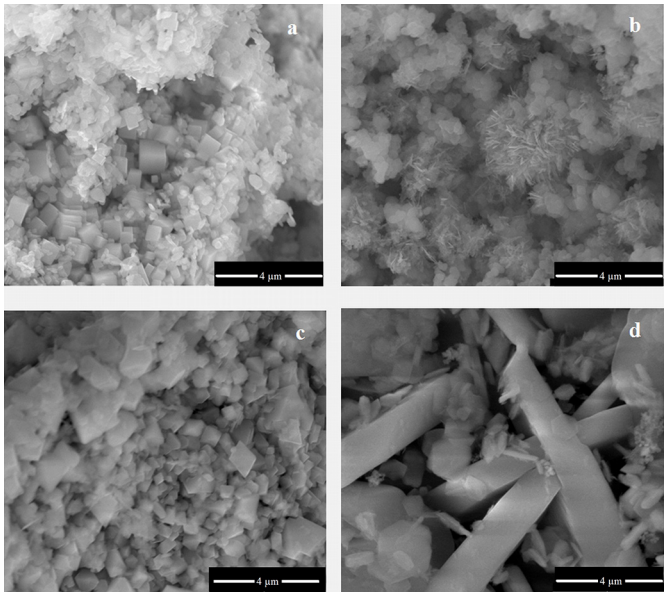

Fig. 2. Scanning electron microscopy images for (a) $ZnTa_2O_6$, (b) $ZnNb_2O_6$, (c) $MgTa_2O_6$ and (d) $MgNb_2O_6$ nanomaterials.

3.2 Optical properties

Using the Kubelka-Munk equations [24,25], the absorbance was calculated for each obtained pseudo-binary oxide nanomaterial. From the absorption spectra (Fig. 5) can be observed the maximum absorption peak for each sample as it follows: 311 nm for $ZnTa_2O_6$, 311 nm for $ZnNb_2O_6$,

Table 2. The calculated S_a and S_q for the measured areas for the obtained nanomaterials.

Nanomaterial	Area (pm^2)	S_a (nm)	S_q(nm)
$ZnTa_2O_6$	1.30	0.09	0.13
$ZnNb_2O_6$		0.13	0.17
$MgTa_2O_6$		0.14	0.22
$MgNb_2O_6$		0.17	0.23

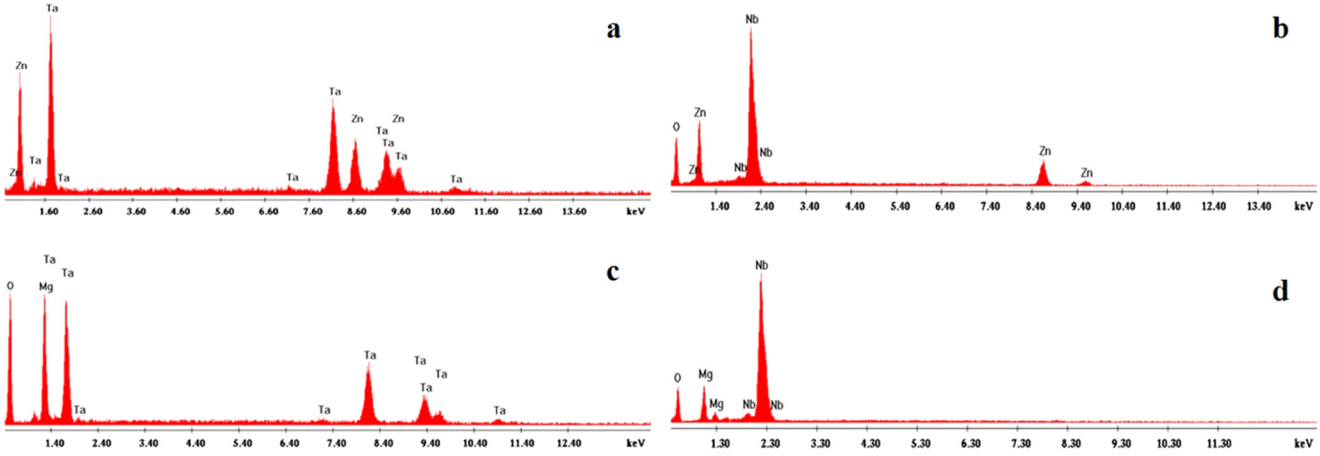

Fig. 3. The EDAX images for (a) $ZnTa_2O_6$, (b) $ZnNb_2O_6$, (c) $MgTa_2O_6$ and (d) $MgNb_2O_6$ nanomaterials.

308 nm for $MgTa_2O_6$ and also 308 nm for $MgNb_2O_6$. The values are the same for the compounds containing Zn and also the same values for the compounds containing Mg, the presence of Nb or Ta does not seems to influence the absorption. Plotting from each of the absorption spectra: $\{(k/s)\,h\nu\}^2$ versus $h\nu$, where k denotes absorption coefficient, s is scattering coefficient and $h\nu$ is the photon energy, the optical band gaps were estimated for the obtained materials as it follows: E_g ($ZnTa_2O_6$) = 3.6 eV, E_g ($ZnNb_2O_6$) = 3.72 eV, E_g ($MgTa_2O_6$) = 3.8 eV and E_g ($MgNb_2O_6$) = 3.76 eV.

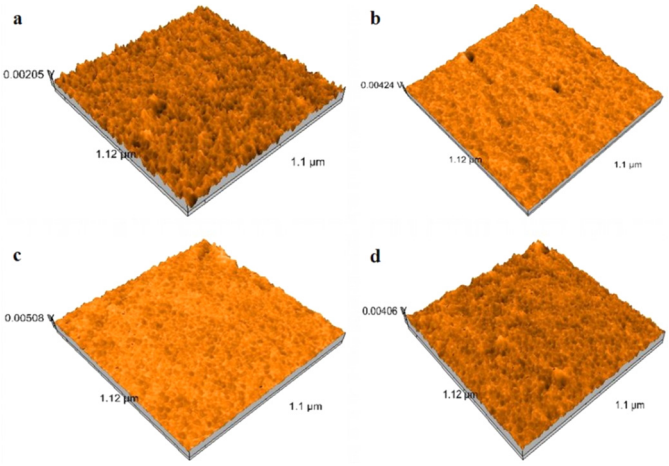

Fig. 4. The atomic force microscopy images of: (a) $ZnTa_2O_6$, (b) $ZnNb_2O_6$, (c) $MgTa_2O_6$ and (d) $MgNb_2O_6$.

3.3 Polarisation curves

In Figure 6 are represented the Tafel plots of the investigated OL electrodes recorded after 30 min open circuit potential (OCP) in 0.5 M Na_2SO_4 solution. The slopes were determined in the Tafel region of the anodic and cathodic curves before and after the corrosion potential (U).

As it can be seen in Table 3, where the calculated parameters from the Tafel plots are summarized, the corrosion potential (E_{corr}) of the OL electrode is −0.916 and the corresponding corrosion current density (i_{corr}) is 24.08 µA/cm^2. The polarization curves were shifted towards the region of lower corrosion current densities in thepresence of $ZnNb_2O_6$ and $MgTaO_6$ and the polarization curves shifted towards the region of higher corrosion current densities in the presence of $ZnTa_2O_6$ and $MgNb_2O_6$.

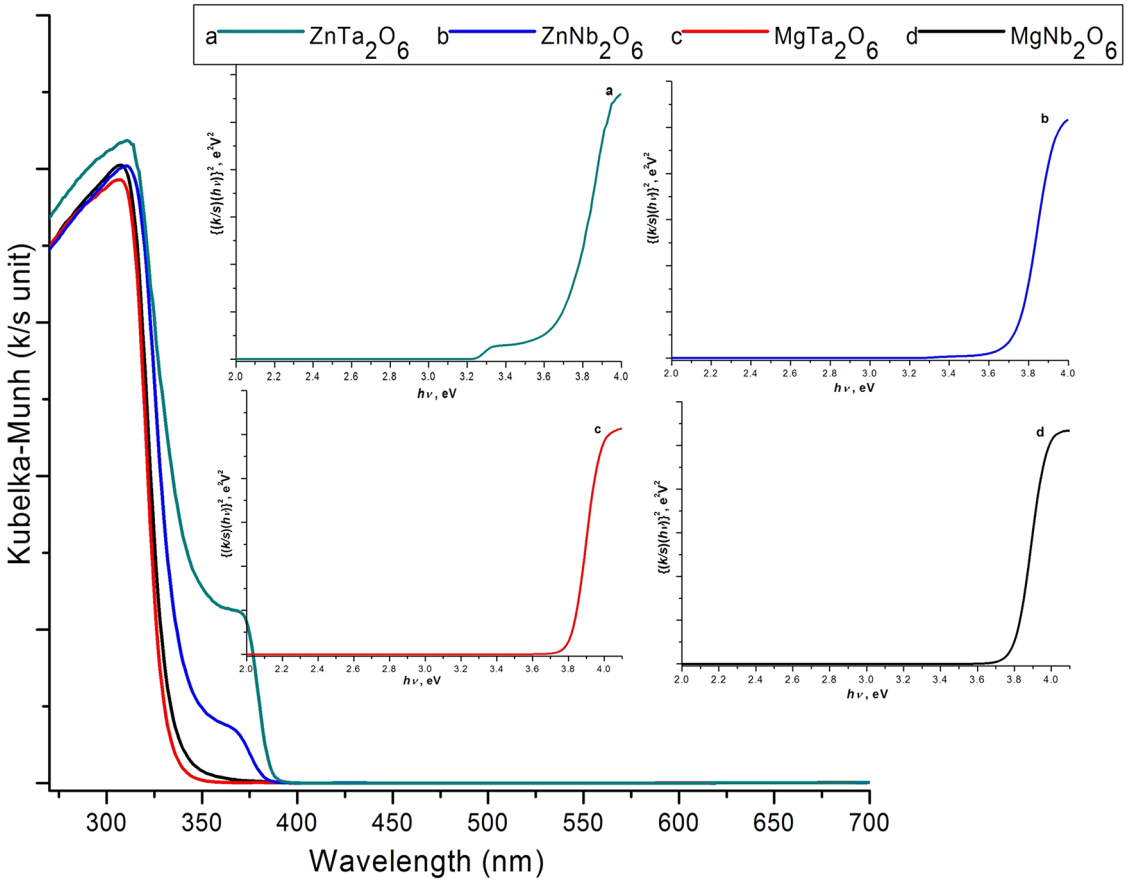

Fig. 5. Absorption spectra of (a) $ZnTa_2O_6$, (b) $ZnNb_2O_6$, (c) $MgTa_2O_6$ and (d) $MgNb_2O_6$ nanomaterials. From the inset plot were obtained the optical band gaps.

Table 3. Tafel parameters of the investigated electrodes after 30 min immersion in 0.5 M Na_2SO_4 solution.

Electrode	E_{corr}/V	i_{corr}/μA cm^{-2}	Rp/kΩ · cm^2	v_{cor}/μm Y^{-1}	IE/%
Bare OL	–0.916	24.08	1.53	104.1	–
$ZnTa_2O_6$	–0.908	10.53	1.98	45.54	56.27
$ZnNb_2O_6$	–0.922	15.17	1.31	65.59	37
$MgTa_2O_6$	–0.921	11.73	1.93	50.74	51.28
$MgNb_2O_6$	–0.910	9.83	2.36	42.52	59.17

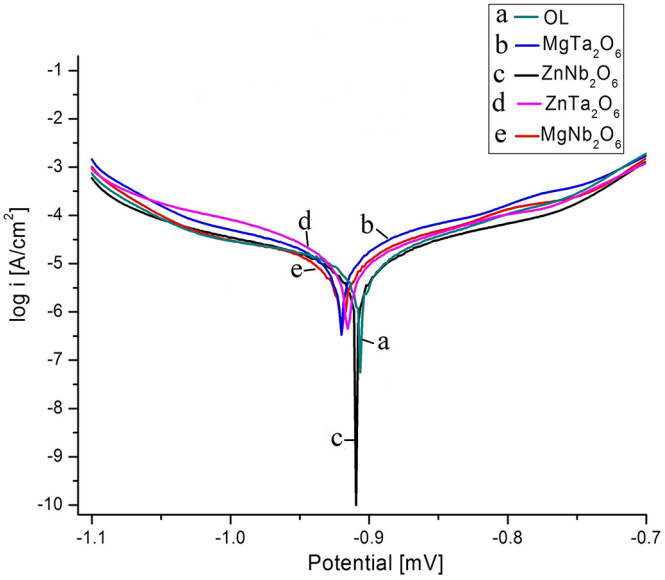

Fig. 6. Tafel representation of polarization curves recorded in 0.5 M Na_2SO_4 for the studied electrodes: (a) OL, (b)$MgTa_2O_6$, (c) $ZnNb_2O_6$, (d) $ZnTa_2O_6$ and (e) $MgNb_2O_6$.

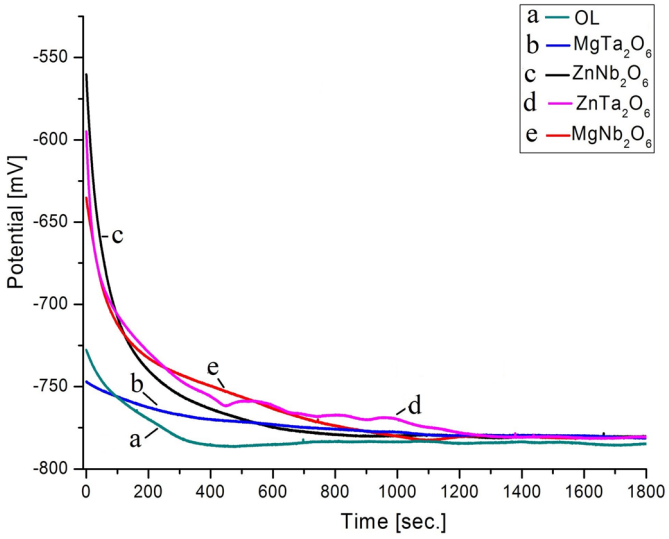

Fig. 7. Evolution of open circuit potential with time for investigated electrodes in 0.5 M Na_2SO_4 electrolyte solution for: (a) OL, (b)$MgTa_2O_6$, (c) $ZnNb_2O_6$, (d) $ZnTa_2O_6$ and (e) $MgNb_2O_6$.

The inhibition efficiencies ($IE\%$) were calculated based on equation (3) from [26] and for: $ZnTa_2O_6$, $MgTa_2O_6$ and $MgNb_2O_6$ were obtained values of $IE\%$ over 50% (see Tab. 3).

$$IE\% = \left(1 - \frac{i_{corr}}{i^0_{corr}}\right) \times 100 \quad (3)$$

where i^0_{corr} and i_{corr} are the corrosion current densities in the absence and in the presence of the pseudo-binary oxide nanomaterials deposited as thin layers on carbon steel electrodes.

In the case of $ZnTa_2O_6$, obtained through the hydrothermal method, the $IE\%$ of 56.27% is higher than the reported $IE\%$ of 48.61% for $ZnTa_2O_6$ obtained through the solid state method [10], while in the case of the $ZnNb_2O_6$ obtained through the hydrothermal method, the IE% of 37% is lower than for the $ZnNb_2O_6$ obtained through the solid state method (52.70%) [10].

The polarization resistance (Rp) increases from 1.53 kΩ cm^2 for bare OL to 2.36 kΩ cm^2 for $MgNb_2O_6$,while in the case of $ZnNb_2O_6$ the value of Rp is decreasing to 1.31 kΩ cm^2 which also reflects in the IE which is only 37%.

Analyzing the evolution of open circuit potential (OCP) with time for the investigated electrodes (Fig. 7), it can be seen that an exposure time of 30 min leads to a shift in free potential towards more negative values. Comparing the OCP profiles, it can be observed that in almost 20 min, the profile of the untreated electrode presents a decrease in potential until it reaches at the same value as for: $ZnNb_2O_6$, $MgTaO_6$ and $MgNb_2O_6$.

4 Conclusion

$ZnTa_2O_6$, $ZnNb_2O_6$, $MgTa_2O_6$ and $MgNb_2O_6$ pseudo-binary oxide nanomaterials were obtained through the hydrothermal synthesis method at 250 °C for 12 h. XRD results reveal that the single phase of the obtained pseudo-binary oxide nanomaterials can be obtained through the hydrothermal synthesis at a pH value of 13. The optical band gaps were estimated from the diffuse reflectance spectrum of each materials to be in the range 3.6–3.8 eV. The inhibition efficiency for the obtained materials was calculated and for $ZnTa_2O_6$, $MgTa_2O_6$ and $MgNb_2O_6$ nanomaterials were obtained values of $IE\%$ over 50%. Taking into consideration that the tested materials

containing Zn and Mg in combination with Ta and Nb did not completely satisfied our expectations, we believe that a further approach using materials containing Mn in combination with Ta and Nb will add a benefit to the efficiency of corrosion, as it was already reported in [27,28].

This work was partially financially supported by the project PN III nr. 107 PED / 2017 "Nanostructured anticorrosive hybrid materials based on pseudo-binary oxides and Zn-metalloporphyrins", partially financially supported as part of the PN 16-14 02 03 and partially project PN III "Hybrid ceramics/porphyrins, deposited by pulsed laser deposition as single and sandwich layers for corrosion inhibition of steels in acid environment".
This paper was presented at the 3rd International Conference "Emerging Technologies in Materials Engineering EmergeMAT", organized by the National R&D Institute for Non-ferrous and Rare Metals – IMNR, Romania, 29–30 October 2020.

References

1. M. Birdeanu, M. Vaida, A.V. Bîrdeanu, E Fagadar-Cosma, Corrosion **76** (2020) 8
2. A.V. Bîrdeanu, D.S. Milovanovic, J. Ciganovic, S. Petronic, M. Vaida, M. Birdeanu, Adv. Mater. Res. **1153** (2019) 3
3. M. Vaida, M. Birdeanu, A.-V Bîrdeanu, AIP Conf. Proc. **2071** (2019) 1
4. A. Batah, H. Chebli, M. Blekhaouda, L. Bammou, R. Salhi, A. Anejjar, B. Chebli, M. Zaafrani, Appl. J. Environ. Eng. Sci. **4** (2017) 3
5. H. Chebli, A. Batah, A. Asdadi, M. Zaafrani, L.M.I. Hassani, S. Bounimi, B. Chebli, Appl. J. Environ. Eng. Sci. **3** (2017) 2
6. A. Hamdouch, A. Anejjar, B. Chebli, L.M.I. Hassani, Appl. J. Environ. Eng. Sci. **3** (2017) 3
7. M. Birdeanu, A.-V. Bîrdeanu, E. Fagadar-Cosma, C. Enache, I. Miron, I. Grozescu, Dig. J. Nanomater. Bios. **8** (2013) 1
8. M. Birdeanu, A.V. Bîrdeanu, M. Vaida, D. Milovanovic, A. Lascu, E. Fagadar-Cosma, Phys. Scr. **94** (2019) 7
9. L.L. Noto, M.L. Chitambo, O.M. Ntwaeaborwa, H.C. Swart, Powder Tech. **247** (2013) 10
10. M. Birdeanu, G. Fagadar-Cosma, I. Sebarchievici, A.–V. Bîrdeanu, B. Taranu, I. Taranu, E. Fagadar-Cosma, J. Serb. Chem. Soc. **81** (2016) 2
11. L.L. Noto, W.D. Roos, O.M. Ntwaeaborwa, M. Gohain, M.Y. A. Yagoub, E. Coetsee, H.C. Swart, Sci. Adv. Mater. **7** (2015) 6
12. L.L. Noto, S.K.K. Shaat, D. Poelman, P.F. Smet, L. Martin, M.Y.A. Yagoub, S.M. Dhlamini, O.M. Ntwaeaborwa, H.C. Swart, Ceram. Int. **42** (2016) 4
13. Z. Ding, W. Wu, S. Liang, H. Zheng, L. Wu, Mater. Lett. **65** (2011) 3
14. A.K. Ganguli, S. Nangia, M, Thirumal, P. Gai, J. Chem. Sci. **118** (2006) 1
15. V. Shanker, A.K. Ganguli, Bull. Mater. Sci. **26** (2003) 7
16. E.R. Camargo, E. Longo, E.R. Leite, J. Sol-Gel Sci. Tech. **17** (2000) 1
17. A.-V. Bîrdeanu, M. Birdeanu, E. Fagadar-Cosma, J. Alloys Compd. **706** (2017) 6
18. N. Shahgholi, K. Asadian, T. Ebadzadeh, Ceram. Int. **40** (2014) 9
19. S. Astorg, S. Marinel, Ceram. Int. **33** (2007) 2
20. S. Chen, Y. Qi, G. Liu, J. Yang, F. Zhang, C. Li, Chem. Commun. **50** (2014) 11
21. M. Birdeanu, M. Vaida, E. Fagadar-Cosma, J. Chem. **2015** (2015) Article ID 752089
22. M. Birdeanu, A.-V. Bîrdeanu, A.S. Gruia, E. Fagadar-Cosma, C.N. Avram, J. Alloys Compd. **573** (2013)
23. V. Kapaklis, P. Poulopoulos, V. Karoutsos, Th. Manouras, C. Politis, Thin Solid Films **510** (2006) 2
24. P. Kubelka, F. Munk, An article on optics of paint layers, Zh. Tekh. Fiz. **12** (1931) 753
25. P. Kubelka, New contributions to the optics of intensely light-scattering materials. Part I, J. Opt. Soc. Am. **38** (1948) 5
26. Z. Ahmad, Principles of Corrosion Engineering and Corrosion Control, Butterworth – Heinemann /IChemE Series. Elsevier, Amsterdam. 2006, p. 377
27. B. Kim, S. Kim, H.S. Kim, Adv. Mater. Sci. Eng. **2018** (2018) Article ID 7638274
28. l. Xiaoyan, L. Mingzhao, F. Liuqun, W. Haiyan, F. Chong, M. Hua, Rare Metal Mat. Eng. **43** (2014) 2

Cite this article as: Mihaela Birdeanu, Mirela Vaida, Eugenia Fagadar-Cosma, Hydrothermal synthesis of $ZnTa_2O_6$, $ZnNb_2O_6$, $MgTa_2O_6$ and $MgNb_2O_6$ pseudo-binary oxide nanomaterials with anticorrosive properties, Manufacturing Rev. **7**, 39 (2020)